LETTER

doi:10.1038/nature11658

DNA-repair scaffolds dampen checkpoint signalling by counteracting the adaptor Rad9

Patrice Y. Ohouo[1], Francisco M. Bastos de Oliveira[1], Yi Liu[1], Chu Jian Ma[1] & Marcus B. Smolka[1]

In response to genotoxic stress, a transient arrest in cell-cycle progression enforced by the DNA-damage checkpoint (DDC) signalling pathway positively contributes to genome maintenance[1]. Because hyperactivated DDC signalling can lead to a persistent and detrimental cell-cycle arrest[2,3], cells must tightly regulate the activity of the kinases involved in this pathway. Despite their importance, the mechanisms for monitoring and modulating DDC signalling are not fully understood. Here we show that the DNA-repair scaffolding proteins Slx4 and Rtt107 prevent the aberrant hyperactivation of DDC signalling by lesions that are generated during DNA replication in *Saccharomyces cerevisiae*. On replication stress, cells lacking Slx4 or Rtt107 show hyperactivation of the downstream DDC kinase Rad53, whereas activation of the upstream DDC kinase Mec1 remains normal. An Slx4–Rtt107 complex counteracts the checkpoint adaptor Rad9 by physically interacting with Dpb11 and phosphorylated histone H2A, two positive regulators of Rad9-dependent Rad53 activation. A decrease in DDC signalling results from hypomorphic mutations in *RAD53* and *H2A* and rescues the hypersensitivity to replication stress of cells lacking Slx4 or Rtt107. We propose that the Slx4–Rtt107 complex modulates Rad53 activation by a competition-based mechanism that balances the engagement of Rad9 at replication-induced lesions. Our findings show that DDC signalling is monitored and modulated through the direct action of DNA-repair factors.

Slx4 is an evolutionarily conserved DNA-repair scaffolding protein that is important for the cellular response to exogenous DNA-damaging agents[4–7], and mutations in human *SLX4* were recently linked to Fanconi anaemia[8,9]. In *S. cerevisiae* (budding yeast), cells that lack *SLX4* (*slx4*Δ cells) are highly sensitive to methyl methanesulphonate (MMS)[7], a DNA-alkylating agent that blocks replication and induces the DDC pathway. While investigating the activation status of the *S. cerevisiae* DDC kinase Rad53 in *slx4*Δ cells, we noted that MMS treatment leads to hyperphosphorylation, and thus hyperactivation, of Rad53 compared with in wild-type cells (Fig. 1a and Supplementary Fig. 1a), which is consistent with a previous report[10]. However, the phosphorylation of histone H2A (also known as Hta1 and Hta2), a substrate of the upstream DDC kinase Mec1, at serine 129 (here referred to as $H2A^{PS129}$) was not increased in *slx4*Δ cells (Fig. 1a, lower panel). These results suggest that the hyperactivation of Rad53 in *slx4*Δ cells is not caused by increased damage-induced Mec1 signalling but by improper downstream regulation of Rad53 activation. To test this possibility, we compared the phosphoproteome of wild-type and *slx4*Δ cells after MMS treatment, using quantitative mass spectrometry. Although most of the detected Mec1 targets were phosphorylated to the same extent in both cell types, Rad53-dependent phosphorylation was significantly higher in *slx4*Δ cells than in wild-type cells (Supplementary Fig. 1b), further supporting the idea that Slx4 has a role in specifically blocking Rad53 hyperactivation. Because the activation of Rad53 in response to MMS mostly depends on the checkpoint adaptor Rad9 (Fig. 1b and Supplementary Fig. 2), Slx4 probably counteracts Rad9-dependent Rad53 activation.

To test whether the sensitivity of *slx4*Δ cells to MMS is caused mostly by aberrant Rad53 hyperactivation, we used hypomorphic alleles of *rad53* that result in lower Rad53 activation, reasoning that these alleles would rescue the MMS sensitivity of *slx4*Δ cells. Rad53 has two FHA domains, which bind to phosphorylated Rad9 in a redundant manner and mediate Rad53 activation[11] (Fig. 1c). Mutations in the FHA2 domain promote a stronger reduction in MMS-induced Rad53 activation than do mutations in the FHA1 domain[12]. Whereas a mutation (R70A, in which arginine is substituted with alanine at amino acid 70) in the FHA1 domain of Rad53 had no effect on the MMS sensitivity of *slx4*Δ cells, a mutation (R605A) in the FHA2 domain reduced the MMS sensitivity of *slx4*Δ cells (Fig. 1d). Consistent with our hypothesis that Rad53 hyperactivation is the cause of the MMS sensitivity of *slx4*Δ cells, mutation of the FHA2 domain resulted in a decrease in Rad53 activation in *slx4*Δ cells to a level similar to that of wild-type cells (Fig. 1e). Collectively, these results suggest that Slx4 has a crucial role in preventing excessive Rad9-dependent activation of Rad53 (Fig. 1f). The levels of MMS used here require that cells pass through the S phase of the cell cycle for Rad53 to become active[13]; therefore, our results suggest that Slx4 counteracts the Rad9–Rad53 pathway in response to replication-induced lesions. The finding that combined deletion of the *SLX1* and *RAD1* genes, which encode nucleases that are known to associate with Slx4, leads to lower MMS sensitivity and Rad53 activation than in *slx4*Δ cells (Supplementary Fig. 4) supports a nuclease-independent function for Slx4 during the cellular response to MMS-induced replication stress.

We recently reported that on replication stress, Slx4 binds to Dpb11 (ref. 14), a replication factor that is involved in DDC activation[15,16]. Because Dpb11 binds to Rad9 and positively regulates Rad9-dependent Rad53 activation[17,18], we assessed whether the Slx4–Dpb11 interaction has a role in counteracting Rad53 activation during MMS treatment. We previously showed that phosphorylation of Slx4 by Mec1 mediates the interaction of Slx4 with Dpb11 and that an Slx4 mutant lacking seven Mec1 consensus phosphorylation sites (Slx4-7MUT) cannot stably interact with Dpb11 (ref. 14). Rad53 is hyperactivated in *slx4-7MUT* cells (Fig. 2a), supporting a model in which the Slx4–Dpb11 interaction is important for preventing Rad53 hyperactivation.

Next, we tested whether the Slx4–Dpb11 interaction inhibits the ability of Rad9 to bind to Dpb11 in wild-type and *slx4*Δ cells. Deletion of *SLX4* leads to a significant increase in the MMS-induced interaction between Dpb11 and Rad9 (Fig. 2b and Supplementary Fig. 5), suggesting that Slx4 and Rad9 compete for Dpb11 binding. Dpb11 contains two pairs of BRCT domains, which bind to phosphorylated motifs. We found that recombinant BRCT domains 1 and 2 ($BRCT^{1/2}$) of Dpb11 can bind phosphorylated Slx4 and phosphorylated Rad9 from MMS-treated *S. cerevisiae* lysates (Fig. 2c). This finding is consistent with a model in which Slx4 and Rad9 compete for $BRCT^{1/2}$ binding.

Dpb11 $BRCT^{1/2}$ was previously shown to interact directly with cyclin-dependent kinase (CDK)-dependent phosphorylation sites in Sld3, thereby initiating DNA replication[19,20]. To better understand the mechanism of the Slx4–Dpb11 interaction, we searched for a

[1]Department of Molecular Biology and Genetics, Weill Institute for Cell and Molecular Biology, Cornell University, Ithaca, New York 14853, USA.

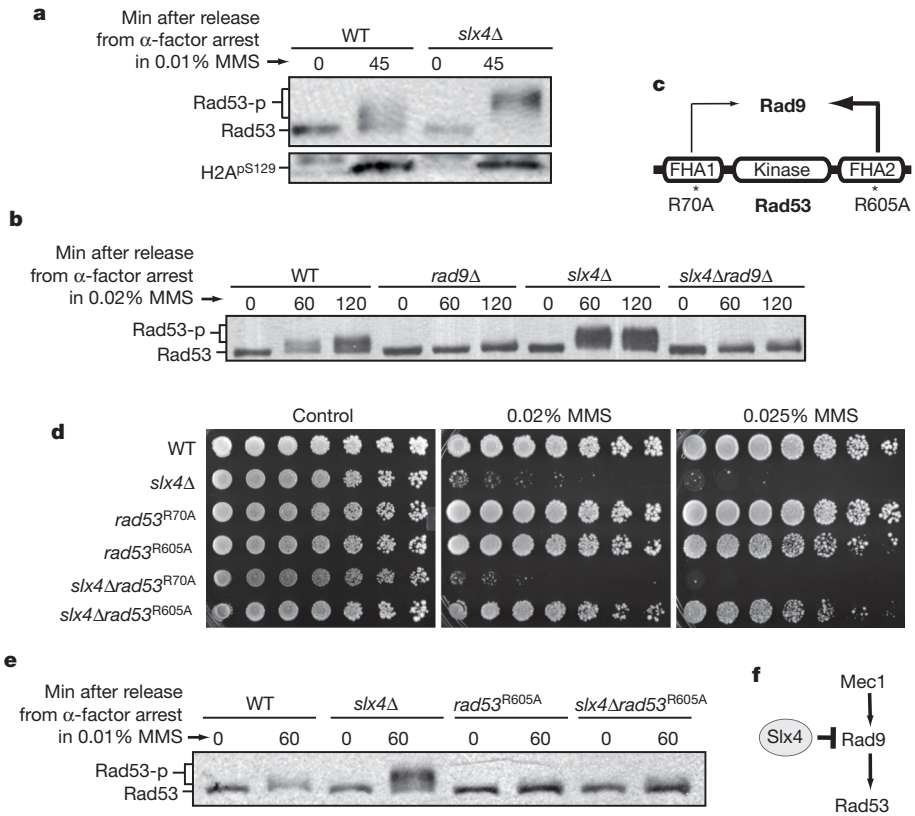

Figure 1 | Slx4 counteracts Rad9-dependent Rad53 activation. **a**, Western blot showing phosphorylation of haemagglutinin (HA)-tagged Rad53 and histone $H2A^{pS129}$ after MMS treatment. **b**, Western blot showing the phosphorylation status of Rad53–HA in the indicated strains after MMS treatment. **c**, Schematic representation of the Rad53 protein and its interaction with Rad9. **d**, MMS sensitivity assay of strains containing the indicated Flag-tagged mutant Rad53 proteins. Similar results were obtained with strains containing untagged Rad53 (Supplementary Fig. 3). **e**, Western blot showing the phosphorylation status of Rad53–Flag in the indicated strains after MMS treatment. **f**, Model for the role of Slx4 in uncoupling Rad53 activation from Mec1 signalling, through counteracting Rad9. Rad53-p, phosphorylated Rad53; WT, wild type.

CDK-targeting motif in Slx4 that resembles the Dpb11-binding region in Sld3. Notably, Slx4 contains proline-directed phosphorylation sites that align well with serine 600 (S600) and S622 of Sld3, which are important for the Dpb11–Sld3 interaction[19,20] (Supplementary Fig. 6). We tested the importance of the proline-directed sites within the Sld3-like region of Slx4 and found that S486 of Slx4 is crucial for the MMS-induced interaction with Dpb11 (Fig. 2d). In addition, three canonical Mec1 phosphorylation sites (S/T-Q sites) that are important for mediating a robust Slx4–Dpb11 interaction[14] are located in or near the Sld3-like Dpb11-binding region in Slx4. We conclude that the Slx4–Dpb11 interaction is mediated by the coordinated action of both Mec1 and a proline-directed kinase at a motif that is probably targeted by BRCT[1/2] of Dpb11. Although we detected residual binding between Dpb11 and Slx4-7MUT, we did not detect an interaction between Dpb11 and $Slx4^{S486A}$, suggesting that the phosphorylation of S486 has a more important role in mediating the Slx4–Dpb11 interaction than the Mec1 consensus phosphorylation sites. This is also supported by the finding that $slx4^{S486A}$ leads to Rad53 hyperactivation (Fig. 2e) and to a higher MMS sensitivity than does *slx4-7MUT* (Fig. 2f). Interestingly, previous reports showed that proline-directed sites in Rad9 are also important for the Dpb11–Rad9 interaction[17,18] (Supplementary Fig. 7).

To further test the model that Slx4 antagonizes Rad53 activation by binding to Dpb11 and outcompeting Rad9, we overexpressed Slx4 using an *ADH1* or a *TDH3* promoter and monitored different steps of checkpoint activation. In an early step in checkpoint activation, Rad9 assembles into a ternary complex with Dpb11 and Mec1 and is hyperphosphorylated by Mec1 (ref. 18). We first monitored the phosphorylation status of Rad9 in cells expressing Slx4 from its endogenous promoter and in cells overexpressing Slx4. Overexpression of wild-type Slx4 but not S486A mutated Slx4 significantly inhibited the MMS-induced hyperphosphorylation of Rad9 (Fig. 2g), as shown by the strong decrease in the slower migrating band at 45 and 60 min after release from α-factor arrest. We then monitored the effect of Slx4 overexpression on Rad53 activation in response to MMS treatment (Supplementary Fig. 8a). Although overexpression of Slx4 leads to a small but consistent decrease in Rad53 activation early in the response, we did not observe the same effect at later time points. We speculated that after 40 min, the Rad53 activation that was observed in Slx4-overexpressing cells was being mediated by a parallel mechanism based on Dot1-mediated histone H3K79 methylation, which can promote the recruitment of Rad9 to lesion sites independently of Dpb11 (ref. 21). We therefore monitored Rad53 activation in cells lacking *DOT1* and found that Slx4 overexpression significantly reduces Rad53 activation also at later time points (Fig. 2h); this effect depends on S486 of Slx4 (Supplementary Fig. 8b, c). Next, we determined whether Slx4 overexpression specifically disrupts the Rad9–Dpb11 interaction. We detected hyperphosphorylated Rad9 in a Dpb11 pull-down from cells expressing Slx4 from its endogenous promoter, but we did not detect Rad9 in a Dpb11 pull-down using cells that overexpressed Slx4 (Fig. 2i). This effect was specific for S486 of Slx4. These findings support our model that Slx4 counteracts DDC signalling by binding to Dpb11 and preventing its stable interaction with Rad9 (Fig. 2j).

Slx4 forms a tight complex with the BRCT-domain-containing protein Rtt107, which is a DNA-repair scaffold that stabilizes the Slx4–Dpb11 interaction[14]. Analysis of the phosphorylation status of Rad53 in *rtt107*Δ cells showed that DDC signalling is hyperactivated (Fig. 3a), suggesting that Rtt107 has a similar function to Slx4 in counteracting

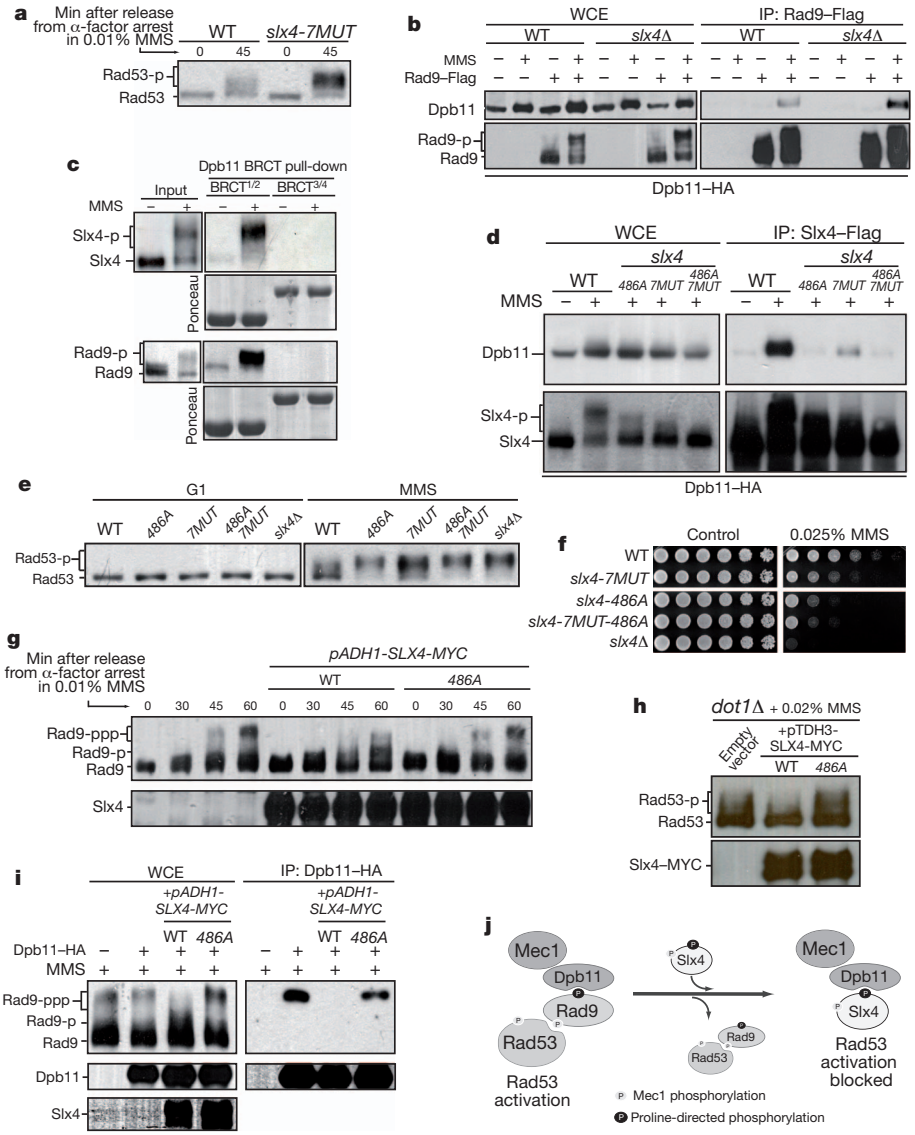

Figure 2 | Slx4 binding to Dpb11 counteracts the Dpb11–Rad9 interaction and Rad53 activation. **a**, Western blot showing the phosphorylation status of Rad53–HA in the indicated strains after MMS treatment. **b**, Co-immunoprecipitation (co-IP) of Dpb11 and Rad9 (see also Supplementary Fig. 5); input levels and phosphorylation status of Rad9 are shown. **c**, Pull-down of Slx4–Flag or Rad9–HA from *S. cerevisiae* lysates using recombinant $BRCT^{1/2}$ and $BRCT^{3/4}$ from Dpb11; ponceau staining of the membrane is also shown. **d**, Interaction of the indicated Flag-tagged Slx4 mutants with Dpb11–HA; input levels and phosphorylation status of Slx4 are shown. **e**, Rad53 phosphorylation status in the indicated *slx4* mutants. The experiment was performed as described in Fig. 1a. **f**, MMS sensitivity assay on the indicated *slx4* mutants. **g**, Rad9 phosphorylation status in cells expressing WT or mutant Slx4 from the endogenous *SLX4* promoter or the *ADH1* promoter. **h**, Rad53 phosphorylation status in *dot1*Δ cells expressing Slx4 from the endogenous *SLX4* promoter or the *TDH3* promoter. Cells were arrested in α-factor and released for 45 min in medium containing MMS. **i**, Co-IP of Dpb11 and Rad9. **j**, Model for the mechanism by which Slx4 counteracts Rad53 activation. G1, G1 cell-cycle phase; Rad9-p, hypophosphorylated Rad9; Rad9-ppp, hyperphosphorylated Rad9; WCE, whole cell extract.

Rad53 activation. Rtt107 recognizes $H2A^{pS129}$ through its carboxy-terminal pair of BRCT domains ($BRCT^{5/6}$), and this region is essential for the role of Rtt107 in the MMS response[22] (Supplementary Figs 9 and 10). Furthermore, the S129A mutation (*h2a-S129A*) abrogated Slx4 phosphorylation on MMS treatment (Fig. 3b), suggesting that the recruitment of Rtt107 to $H2A^{pS129}$ occurs upstream of Slx4–Dpb11 complex formation. Because $H2A^{pS129}$ can function as a positive regulator of Rad9-dependent Rad53 activation[23], we reasoned that the hyperactivation of Rad53 in *rtt107*Δ cells could be suppressed by *h2a-S129A*. *rtt107*Δ cells expressing the H2A(S129A) mutant had lower Rad53 activation and MMS sensitivity than did *rtt107*Δ cells expressing wild-type H2A (Fig. 3c, d). Disruption of the Rad9–H2A interaction by mutation of the C-terminal pair of BRCT domains of Rad9 (K1088M) partially rescued the MMS sensitivity of *rtt107*Δ cells (Supplementary Fig. 11a). A similar rescue was also observed when overexpressing $BRCT^{5/6}$ of Rtt107 (Supplementary Fig. 11b). Taken together, these results show that, like Slx4, Rtt107 also counteracts DDC signalling. The anti-checkpoint function of Rtt107 depends on its recognition of $H2A^{pS129}$, a step that is required subsequently for the assembly of the Slx4–Dpb11 complex. Thus, the Slx4–Rtt107 complex functions as a negative regulator of activation of the kinase Rad53 by physically interacting with two positive regulators of the adaptor Rad9: Dpb11 and $H2A^{pS129}$.

To further test the anti-checkpoint function of the Slx4–Rtt107 complex, we developed an alternative experimental set-up in which the presence of Slx4 would sensitize cells to replication stress by decreasing DDC signalling below the level required for a proper cellular response. For this set-up, we used cells lacking Mrc1, which is a checkpoint adaptor that works in parallel with Rad9. Mrc1 mediates Rad53 activation at stalled replication forks and therefore has a more

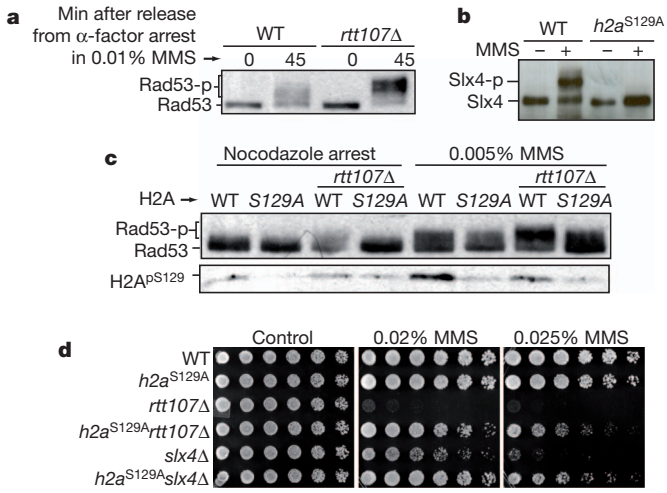

Figure 3 | Rtt107 counteracts Rad9-dependent Rad53 activation by binding to phosphorylated histone H2A. **a**, Western blot showing the phosphorylation status of Rad53–HA in the indicated strains after MMS treatment. **b**, Western blot showing Slx4–Flag phosphorylation status. **c**, Western blot showing phosphorylation status of Rad53 and H2A^{pS129}. Indicated strains expressing HA-tagged Rad53 were arrested in nocodazole and released for 60 min in medium containing MMS. **d**, MMS sensitivity assay on the indicated mutants.

central role than Rad9 in Rad53 activation in response to hydroxyurea[24]. On hydroxyurea treatment, *mrc1*Δ cells rely solely on Rad9 to activate Rad53. The interaction of Slx4 with Dpb11 was enhanced in *mrc1*Δ cells (Fig. 4a), especially in response to hydroxyurea, suggesting that the Slx4–Rtt107 complex actively counteracts Rad9 in *mrc1*Δ cells (Fig. 4b). Consistent with our finding that the Slx4–Dpb11 interaction requires H2A^{pS129}, high levels of H2A^{pS129} accumulated close to the origins of replication in *mrc1*Δ cells after hydroxyurea treatment (Fig. 4c). Because we expect that the kinase activity of Rad53 is limiting in *mrc1*Δ cells, we reasoned that deletion of *SLX4* would be beneficial in hydroxyurea-treated *mrc1*Δ cells, allowing more activation of

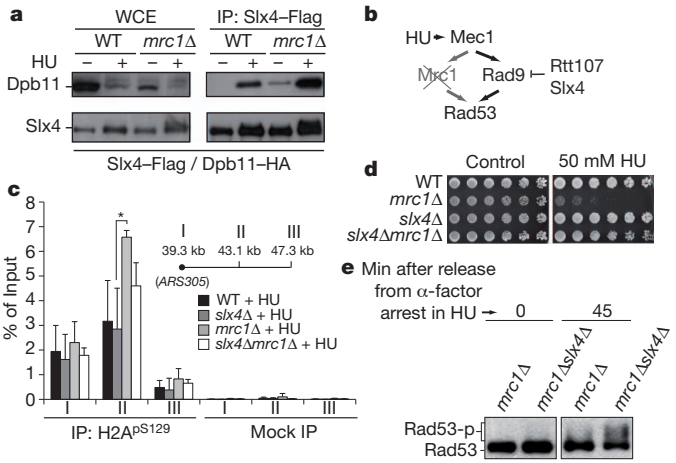

Figure 4 | Slx4 sensitizes *mrc1*Δ cells to hydroxyurea-induced replication stress. **a**, Co-IP of Dpb11 and Slx4 after 2 h treatment with 0.1 M hydroxyurea (HU). **b**, Model for the action of Slx4 and Rtt107 in *mrc1*Δ cells. **c**, HU treatment of *mrc1*Δ cells leads to H2A^{pS129} accumulation near an origin of replication. Chromatin immunoprecipitation (ChIP) analysis of H2A^{pS129} at neighbouring *ARS305* regions I, II and III in the indicated strains after exposure to 0.2 M HU. Data are presented as mean + s.e.m. ($n = 3$). *, significant difference ($P = 0.025$), as analysed by unpaired, two-tailed student's *t*-test. **d**, HU sensitivity assay on the indicated mutants. **e**, Western blot showing the phosphorylation status of Rad53–HA after treatment with 10 mM HU. kb, kilobases.

Rad53 through Rad9. Consistent with this idea, *mrc1*Δ*slx4*Δ cells had a significantly higher hydroxyurea resistance than *mrc1*Δ cells (Fig. 4d), and this resistance correlated with higher Rad53 activation (Fig. 4e). Taken together, these results show that Slx4 sensitizes *mrc1*Δ cells to replication stress, and they provide strong additional evidence that the Slx4–Rtt107 complex counteracts Rad9 in response to replication-induced lesions (see detailed model in Supplementary Fig. 12). Because this function of the Slx4–Rtt107 complex depends on Mec1-dependent phosphorylation, we propose that Slx4–Rtt107 is involved in a mechanism that we have named DAMP — dampens checkpoint adaptor-mediated phospho-signalling — by which DDC signalling self-monitors its activation state. We speculate that by uncoupling upstream Mec1 signalling from downstream Rad53 activation, DAMP could allow Mec1 to maintain control over specific effectors, such as repair enzymes, without an aberrant arrest in cell-cycle progression.

METHODS SUMMARY

The yeast strains and plasmids used are described in Supplementary Tables 3 and 4. The mass-spectrometry-based phosphorylation analyses of whole cell lysates or purified Rad53, as well as the other procedures used for cell growth and synchronization, genotoxin treatment and chromatin immunoprecipitation analysis, are detailed in the Methods.

Full Methods and any associated references are available in the online version of the paper.

Received 18 August 2011; accepted 4 October 2012.
Published online 18 November 2012.

1. Weinert, T. A. & Hartwell, L. H. The *RAD9* gene controls the cell cycle response to DNA damage in *Saccharomyces cerevisiae*. *Science* **241,** 317–322 (1988).
2. Clerici, M. *et al.* Hyperactivation of the yeast DNA damage checkpoint by *TEL1* and *DDC2* overexpression. *EMBO J.* **20,** 6485–6498 (2001).
3. Pellicioli, A., Lee, S. E., Lucca, C., Foiani, M. & Haber, J. E. Regulation of *Saccharomyces* Rad53 checkpoint kinase during adaptation from DNA damage-induced G2/M arrest. *Mol. Cell* **7,** 293–300 (2001).
4. Fekairi, S. *et al.* Human SLX4 is a Holliday junction resolvase subunit that binds multiple DNA repair/recombination endonucleases. *Cell* **138,** 78–89 (2009).
5. Svendsen, J. M. *et al.* Mammalian BTBD12/SLX4 assembles a Holliday junction resolvase and is required for DNA repair. *Cell* **138,** 63–77 (2009).
6. Muñoz, I. M. *et al.* Coordination of structure-specific nucleases by human SLX4/BTBD12 is required for DNA repair. *Mol. Cell* **35,** 116–127 (2009).
7. Fricke, W. M. & Brill, S. J. Slx1–Slx4 is a second structure-specific endonuclease functionally redundant with Sgs1–Top3. *Genes Dev.* **17,** 1768–1778 (2003).
8. Stoepker, C. *et al.* SLX4, a coordinator of structure-specific endonucleases, is mutated in a new Fanconi anemia subtype. *Nature Genet.* **43,** 138–141 (2011).
9. Kim, Y. *et al.* Mutations of the *SLX4* gene in Fanconi anemia. *Nature Genet.* **43,** 142–146 (2011).
10. Roberts, T. M. *et al.* Slx4 regulates DNA damage checkpoint-dependent phosphorylation of the BRCT domain protein Rtt107/Esc4. *Mol. Biol. Cell* **17,** 539–548 (2006).
11. Schwartz, M. F. *et al.* Rad9 phosphorylation sites couple Rad53 to the *Saccharomyces cerevisiae* DNA damage checkpoint. *Mol. Cell* **9,** 1055–1065 (2002).
12. Schwartz, M. F., Lee, S. J., Duong, J. K., Eminaga, S. & Stern, D. F. FHA domain-mediated DNA checkpoint regulation of Rad53. *Cell Cycle* **2,** 381–394 (2003).
13. Tercero, J. A., Longhese, M. P. & Diffley, J. F. A central role for DNA replication forks in checkpoint activation and response. *Mol. Cell* **11,** 1323–1336 (2003).
14. Ohouo, P. Y., Bastos de Oliveira, F. M., Almeida, B. S. & Smolka, M. B. DNA damage signaling recruits the Rtt107–Slx4 scaffolds via Dpb11 to mediate replication stress response. *Mol. Cell* **39,** 300–306 (2010).
15. Navadgi-Patil, V. M. & Burgers, P. M. Yeast DNA replication protein Dpb11 activates the Mec1/ATR checkpoint kinase. *J. Biol. Chem.* **283,** 35853–35859 (2008).
16. Mordes, D. A., Nam, E. A. & Cortez, D. Dpb11 activates the Mec1–Ddc2 complex. *Proc. Natl Acad. Sci. USA* **105,** 18730–18734 (2008).
17. Granata, M. *et al.* Dynamics of Rad9 chromatin binding and checkpoint function are mediated by its dimerization and are cell cycle-regulated by CDK1 activity. *PLoS Genet.* **6,** e1001047 (2010).
18. Pfander, B. & Diffley, J. F. Dpb11 coordinates Mec1 kinase activation with cell cycle-regulated Rad9 recruitment. *EMBO J.* **30,** 4897–4907 (2011).
19. Tanaka, S. *et al.* CDK-dependent phosphorylation of Sld2 and Sld3 initiates DNA replication in budding yeast. *Nature* **445,** 328–332 (2007).
20. Zegerman, P. & Diffley, J. F. Phosphorylation of Sld2 and Sld3 by cyclin-dependent kinases promotes DNA replication in budding yeast. *Nature* **445,** 281–285 (2007).
21. Puddu, F. *et al.* Phosphorylation of the budding yeast 9-1-1 complex is required for Dpb11 function in the full activation of the UV-induced DNA damage checkpoint. *Mol. Cell. Biol.* **28,** 4782–4793 (2008).
22. Li, X. *et al.* Structure of C-terminal tandem BRCT repeats of Rtt107 protein reveals critical role in interaction with phosphorylated histone H2A during DNA damage repair. *J. Biol. Chem.* **287,** 9137–9146 (2012).

23. Javaheri, A. *et al.* Yeast G1 DNA damage checkpoint regulation by H2A phosphorylation is independent of chromatin remodeling. *Proc. Natl Acad. Sci. USA* **103,** 13771–13776 (2006).
24. Alcasabas, A. A. *et al.* Mrc1 transduces signals of DNA replication stress to activate Rad53. *Nature Cell Biol.* **3,** 958–965 (2001).

Supplementary Information is available in the online version of the paper.

Acknowledgements This work was supported by grants from the National Institutes of Health (RO1-GM097272 to M.B.S. and F31-GM093588 to P.Y.O.). F.M.B.O. was supported by a Cornell Fleming Research Fellowship. C.J.M. was supported by an HHMI Institutional Undergraduate Education Grant to Cornell. The authors thank B. Almeida for technical assistance and R. Weiss, S. Emr, A. Bretscher, G. Balmus and P. Russell for comments on the manuscript.

Author Contributions P.Y.O., F.M.B.O. and M.B.S. designed and performed experiments and analysed the data. P.Y.O. and M.B.S. performed the mass spectrometry experiments. F.M.B.O. performed the chromatin immunoprecipitation analysis and generated the *slx4* mutants. Y.L. and P.Y.O. performed co-immunoprecipitations between Dpb11 and Rad9. Y.L. performed pull-down experiments with the BRCT domains of Dpb11. C.J.M. performed the Rtt107–H2A binding assay and the experiments with the Rtt107 BRCT domains. P.Y.O. and M.B.S. performed experiments involving the overexpression of Slx4. P.Y.O. and M.B.S. wrote the paper.

Author Information Reprints and permissions information is available at www.nature.com/reprints. The authors declare no competing financial interests. Readers are welcome to comment on the online version of the paper. Correspondence and requests for materials should be addressed to M.B.S. (mbs266@cornell.edu).

METHODS

Yeast strains and plasmids. Strains generated in this study were derived either from MBS164 or MBS191 (both congenic to S288C) or W303 (where indicated). Unless indicated, all tags were inserted at the C terminus of the corresponding genes by homologous recombination at the genomic loci and were verified by western blotting. Tagged strains were assayed for sensitivity to MMS to ensure they behaved similarly to the wild-type strain. Sensitivity assays were independently confirmed in strains derived from freshly sporulated diploids. Standard cloning methods were used to generate the plasmids for this study. Plasmids containing domains of Dpb11 or Rtt107 tagged at the amino terminus with a PATH tag (2× protein A + TEV cleavage site + 6× His)[25] were based on the pET21a vector (Novagen). HA-tagged full-length Rtt107, together with its native promoter, was cloned into pRS416 (Stratagene) to generate pMBS163. Wild-type alleles cloned into the pFA6a vector (Addgene) were linearized before integration into the respective endogenous loci. A pYES2/NT C vector (Invitrogen) containing full-length or C-terminal BRCTs of Rtt107 was used for overexpression. *SLX4* and *DPB11* constructs containing an *ADH1* or a *TDH3* promoter were generated by fusing the respective promoters (800 base pairs upstream of the start codon) to the corresponding open reading frame. The resultant PCR products were subsequently cloned into the pRS416 or pFA6a vector. All point mutations were generated by site-directed mutagenesis using either the QuikChange Multi Site-Directed Mutagenesis Kit (Stratagene) or the PFU Ultra II kit (Agilent). All yeast strains and plasmids used in this study are described in Supplementary Tables 3 and 4 and are available on request.

Cell synchronization and genotoxin treatment. Yeast cells were grown in yeast peptone dextrose (YPD) or drop-out medium at 30 °C. Log phase cultures (optical density at 600 nm ≈ 0.3) were subjected to α-factor (0.5 μg ml^{-1}) or nocodazole (1.5 μg ml^{-1}) treatment for G1 or G2/M arrest, respectively. Cells were then washed and resuspended in warm medium containing the indicated genotoxin.

Western blotting and immunoprecipitation. For western blotting, about 50 mg frozen cell pellet was lysed by bead beating at 4 °C in lysis buffer (50 mM Tris-HCl, pH 7.5, 0.2% Tergitol, 150 mM NaCl, 5 mM EDTA, 1 mM phenylmethylsulphonyl fluoride (PMSF), Complete, EDTA-free Protease Inhibitor Cocktail (Roche) and PhosSTOP (Roche)). SDS loading buffer with 60 mM dithiothreitol (DTT) was added. Samples were separated by standard SDS-polyacrylamide gel electrophoresis (SDS–PAGE). Proteins were detected using the following antibodies: anti-Rad53 (yc-19, 1:10,000, Santa Cruz Biotechnology), anti H2A^{pS129} (07-0745, 1:10,000, Millipore), anti-HA (12CA5, 1:10,000, Roche) and anti-Flag (M2, 1:5,000, Sigma) antibodies. For immunoprecipitation (IP), approximately 100 mg frozen cell pellet was lysed by bead beating at 4 °C in lysis buffer (50 mM Tris-HCl, pH 7.5, 0.2% Tergitol, 150 mM NaCl, 5 mM EDTA, 1 mM PMSF, Complete, EDTA-free Protease Inhibitor Cocktail, 5 mM sodium fluoride and 10 mM β-glycerophosphate). After adjusting protein concentrations to about 6 mg ml^{-1}, inputs were aliquoted, and lysates were incubated with either anti-HA or anti-Flag agarose resin (Sigma) for 2–3 h at 4 °C. After three washes in lysis buffer, bound proteins were eluted with three resin volumes of SDS elution buffer (100 mM Tris-HCl, pH 8.0, and 1% SDS) for HA IP or of Flag peptide (Sigma) solution (0.5 μg ml^{-1} in 100 mM Tris and 0.2% Tergitol) for Flag IP. SDS loading buffer with DTT was added, and samples were analysed by western blotting with the indicated antibodies.

Pull-down with recombinant BRCT domain. Protein domains (for Dpb11 BRCT$^{1/2}$, amino acids 1–270; and BRCT$^{3/4}$, amino acids 271–582) containing an N-terminal PATH tag (see Yeast strains and plasmids) were expressed in *Escherichia coli*, bound to human IgG–agarose resin (GE Healthcare) and then used as bait for pull-downs from yeast lysates as previously described[25].

SILAC labelling of yeast. For mass spectrometry experiments, cells were grown in (−)Arg (−)Lys drop-out medium ('light' version complemented with normal arginine and lysine; 'heavy' version complemented with lysine $^{13}C_6$, $^{15}N_2$ and arginine $^{13}C_6$, $^{15}N_4$) for at least five generations.

Purification of phosphopeptides by immobilized metal-ion affinity chromatography (IMAC). For the purification of Rad53 phosphopeptides, approximately 0.6 g cell pellet from wild-type (grown in heavy medium) or *slx4*Δ (grown in light medium) strains carrying Rad53–HA was lysed by bead beating at 4 °C in 4 ml lysis buffer (50 mM Tris-HCl, pH 7.5, 0.2% Tergitol, 150 mM NaCl, 5 mM EDTA, Complete, EDTA-free Protease Inhibitor Cocktail, 5 mM sodium fluoride and 10 mM β-glycerophosphate). Lysates were incubated with anti-HA–agarose resin (Sigma) for 4 h at 4 °C. After three washes with lysis buffer, bound proteins were eluted with three resin volumes of elution buffer (100 mM Tris-HCl, pH 8.0, and 1% SDS). Eluted proteins from light or heavy medium were mixed together, reduced, alkylated and precipitated. Proteins were resuspended in a solution of 2 M urea and 12.5 mM Tris-HCl, pH 8.0, and digested with trypsin for 16 h at 37 °C. Phosphopeptides were enriched using an 'in-house' IMAC column, then eluted with 10% ammonia and 10% acetonitrile and dried in a SpeedVac evaporator.

Phosphoproteome analysis. Approximately 0.6 g cell pellet from wild-type (grown in light medium) and *slx4*Δ (grown in heavy medium) strains was lysed by bead beating at 4 °C in 4 ml of lysis buffer (50 mM Tris-HCl, pH 7.5, 0.2% Tergitol, 150 mM NaCl, 5 mM EDTA, Complete, EDTA-free Protease Inhibitor Cocktail (Roche), 5 mM sodium fluoride and 10 mM β-glycerophosphate). Protein lysates were denatured in 1% SDS, reduced, alkylated and then precipitated with three volumes of a solution containing 50% acetone and 50% ethanol. Proteins were solubilized in a solution of 2 M urea, 50 mM Tris-HCl, pH 8.0, and 150 mM NaCl, and then TPCK-treated trypsin was added. Digestion was performed overnight at 37 °C, and then trifluoroacetic acid and formic acid were added to a final concentration of 0.2%. Peptides were desalted with a Sep-Pak C18 column (Waters), dried in a SpeedVac evaporator and resuspended in 1% acetic acid. Phosphopeptides were enriched by IMAC as previously described[26–28], reconstituted in 85 μl solution containing 80% acetonitrile and 1% formic acid, and fractionated by hydrophilic interaction liquid chromatography (HILIC) as previously described[26], before analysis by liquid chromatography with tandem mass spectrometry (LC-MS/MS). More than 3,570 phosphopeptides were identified or quantified, and phosphopeptides containing a phosphorylation site known to be a Mec1 target or a target of Rad53-dependent phosphorylation[27,29] were selected.

Mass spectrometry analysis. IMAC elutions or HILIC fractions were dried in a SpeedVac evaporator, reconstituted in 0.1% trifluoroacetic acid and analysed by LC-MS/MS using a 125 μM ID capillary C18 column and an Orbitrap XL mass spectrometer coupled with an Eksigent nanoflow system. Database searching was performed using the SORCERER system (Sage-N Research) running the program SEQUEST. After searching a target-decoy budding yeast database, results were filtered either based on probability score to achieve a 1% false positive rate or manual inspection. Quantification of heavy/light peptide isotope ratios was performed using the Xpress program as previously described[27].

Chromatin immunoprecipitation (ChIP). Cultures were grown in YPD to an optical density at 600 nm ≈ 0.3, arrested in G1 with α-factor for 2 h and released in the presence of 200 mM hydroxyurea (HU) for 1 h. Cultures were formaldehyde-crosslinked (1% final concentration) for 20 min followed by quenching with 125 mM glycine. Protein–DNA complexes were immunoprecipitated with a yeast-specific anti-phospho-histone (H2A^{pS129}) antibody (07-745, Millipore). Quantitative PCR was performed with the purified DNA from the immunoprecipitate as previously described[30] using pairs of primers designed to amplify the genome sequences shown in Fig. 4c. The primer sequences were as follows: 39.3Kb_for, 5′-CAAGTGG ATTGAGGCCACAGCA-3′, 39.3Kb_rev, 5′-CCGGACAGTACATGAAACT GGACA-3′; 43.1Kb_for, 5′-TCAAGGTGGCTTGATGATCGCC-3′, 43.1Kb_rev, 5′-CACCTCCAATCTGCTTCAAGTTTGGC-3′; 47.3Kb_for, 5′-TATCTTGCG GGCCTTTCGTGTC-3′, and 47.3Kb_rev, 5′-GGGAGATTCCATTTCCGCA CCA-3′.

25. Smolka, M. B. *et al.* An FHA domain-mediated protein interaction network of Rad53 reveals its role in polarized cell growth. *J. Cell Biol.* **175,** 743–753 (2006).
26. Albuquerque, C. P. *et al.* A multidimensional chromatography technology for in-depth phosphoproteome analysis. *Mol. Cell. Proteomics* **7,** 1389–1396 (2008).
27. Smolka, M. B., Albuquerque, C. P., Chen, S. H. & Zhou, H. Proteome-wide identification of *in vivo* targets of DNA damage checkpoint kinases. *Proc. Natl Acad. Sci. USA* **104,** 10364–10369 (2007).
28. Smolka, M. B. *et al.* Dynamic changes in protein–protein interaction and protein phosphorylation probed with amine-reactive isotope tag. *Mol. Cell. Proteomics* **4,** 1358–1369 (2005).
29. Chen, S. H., Albuquerque, C. P., Liang, J., Suhandynata, R. T. & Zhou, H. A proteome-wide analysis of kinase-substrate network in the DNA damage response. *J. Biol. Chem.* **285,** 12803–12812 (2010).
30. Petesch, S. J. & Lis, J. T. Rapid, transcription-independent loss of nucleosomes over a large chromatin domain at *Hsp70* loci. *Cell* **134,** 74–84 (2008).